American Mineralogist, Volume 79, pages 909–920, 1994

TEM-AEM observations of Cl-rich amphibole and biotite and possible petrologic implications

Chen Zhu*
Woods Hole Oceanographic Institution, Woods Hole, Massachusetts 02540, U.S.A.
Huifang Xu**
Department of Earth and Planetary Sciences, The Johns Hopkins University, Baltimore, Maryland 21218, U.S.A.
Eugene S. Ilton
Department of Earth and Environmental Sciences, Lehigh University, Bethlehem, Pennsylvania 18015-3188, U.S.A.
David R. Veblen
Department of Earth and Planetary Sciences, The Johns Hopkins University, Baltimore, Maryland 21218, U.S.A.
Darrell J. Henry
Department of Geology and Geophysics, Louisiana State University, Baton Rouge, Louisiana 70803, U.S.A.
Meg K. Tivey, Geoffrey Thompson
Woods Hole Oceanographic Institution, Woods Hole, Massachusetts 02540, U.S.A.

Abstract

Cl-rich amphibole and biotite (2.9 and 2.8 wt% Cl, respectively) were analyzed with high-resolution transmission electron microscopy (HRTEM), selected-area electron diffraction (SAED), and X-ray emission analytical electron microscopy (AEM). The samples are from Archean granulite-facies metamorphosed iron formations located in the Beartooth Mountains, Montana, U.S.A. Two types of amphibole and biotite were found: (1) high-Cl prograde hastingsite and biotite and (2) retrograde amphibole of grunerite composition containing no detectable amount of Cl but intergrown with submicrometer-sized slabs of Cl-rich annite (2.8 wt%), Fe-rich talc, Fe-rich clinojimthompsonite, and very wide chain silicate.

TEM-AEM study of prograde hastingsite and biotite suggests that Cl is dissolved in the crystal structures and that Cl distribution is homogeneous. AEM analyses show that Cl occupies up to about 30 and 15% of the OH positions in hastingsite and biotite, respectively. Calculations of the Cl-OH exchange reaction for apatite indicate a high $\log(a_{HCl^0}/a_{H_2O})$ ratio of about $-1.8 \sim -2.2$, suggesting equilibrium with a Cl-rich fluid. Speciation and solubility modeling of the equilibrium between an aqueous fluid and the Cl-rich apatite, biotite, and hastingsite suggest that reactions with a saline brine of about 25 wt% NaCl could explain the Cl enrichment in these hydrous phases, whereas the brine may coexist with an immiscible CO_2-dominated vapor during the granulite-facies metamorphism, in light of low calculated H_2O activities and CO_2-rich fluid inclusions. This explanation is consistent with the results from studies of natural and synthetic fluid inclusions and phase equilibrium experiments reported in the literature. The widespread occurrence of Cl-rich amphibole and biotite in granulite-facies rocks thus has significant implications for the nature of high-grade metamorphism.

TEM-AEM observations of submicrometer-sized inclusions of Cl-rich phases within retrograde amphibole may help to explain the commonly observed heterogeneities of electron microprobe Cl analyses, found in samples from a variety of geologic settings. Microprobe analyses using typical beam diameters may sample areas with different proportions of submicroscopic intergrowths. This will give apparent Cl heterogeneities and fortuitous correlations between Cl and concentrations of K, Al, and Si. Although compositional correlations sometimes indicate reciprocal effects that are likely important for amphibole, we emphasize the potential danger of artifacts resulting from submicroscopic solid inclusions. Additional TEM-AEM studies on complex samples are needed to explain the compositional heterogeneities with confidence.

* Present address: GeoTrans, Inc., 4888 Pearl East Circle, Suite 300-E, Boulder, Colorado 80301, U.S.A.
** Present address: Department of Geology, Arizona State University, Tempe, Arizona 85287, U.S.A.

0003–004X/94/0910–0909$02.00

Introduction

In recent years, an increasing number of reports on Cl-rich biotite and amphibole (Dick and Robinson, 1979; Tyler, 1979; Blattner, 1980; Kamineni et al., 1982; Vanko, 1986; Gulyaeva et al., 1986; Suwa et al., 1987; Nash, 1989; Henry, 1990; Valley et al., 1990; Tracy, 1991; Morrison, 1991) have promoted interest in both the crystal chemistry of Cl and the petrologic implications of Cl enrichment in biotite and amphibole. Commonly, it is believed that Cl^- substitutes for OH^- in the crystal structures of hydrous silicates, including biotite and amphibole (e.g., Deer et al., 1966; Brehler and Fuge, 1974). However, this substitution is believed to be limited because the Shannon-Prewitt ionic radius of Cl^- (1.81 Å) is much larger than that of OH^- (1.35 Å). Laboratory synthesis of Cl-rich biotite is difficult. The highest Cl concentration achieved in synthetic annite is about 2 wt% under extremely acidic conditions (Munoz and Swenson, 1981). Therefore, Cl concentrations in natural biotite and amphibole up to 7.15 wt% are intriguing. Intuitively, substitution of the much larger Cl^- ion for OH^- into hydrous silicates should cause lattice strain and possibly local disruption of the crystal structure. In addition, the Cl concentrations of biotite and amphibole grains commonly vary sharply within a single thin section (Henry, 1990; Vanko, 1986; Morrison, 1991). These observations suggest that Cl, at high concentrations, might exist in hydrous silicates in a nonstructural position, for example, as the neutral molecule HCl (Donnay et al., 1978; Volfinger et al., 1985) or as submicroscopic solid inclusions of discrete Cl-rich phases.

To elucidate the crystal chemical behavior of Cl, the use of advanced analytical methods is necessary. Swope et al. (1991) used single-crystal X-ray diffractometry to study the average crystal structure of Cl-rich biotite. Here, we report the results from a high-resolution transmission electron microscopy (HRTEM), selected-area electron diffraction (SAED), and X-ray emission analytical electron microscopy (AEM) study of Cl-rich biotite and amphibole (2.9 and 2.8 wt%, respectively). In addition to the TEM-AEM observations, we also present the results of thermodynamic calculations and use these results to examine the petrologic implications of Cl-OH substitution and Cl enrichment in biotite and amphibole.

Geological setting and sample description

The iron formation sample was collected from Archean granulite-facies rocks at the Quad Creek locality near the eastern border of the Beartooth Mountains, Montana, U.S.A. Geological background and description of the samples are given in detail in Henry et al. (1982), Henry (1990), and Mogk and Henry (1988), and they are only briefly discussed here. The eastern portion of the Beartooth Mountains is dominated by 2.8 billion-year-old granitic to tonalitic granitoids, gneisses, and migmatites. These rocks contain a variety of metasupracrustal inclusions that were metamorphosed to granulite-facies condition at ~3.2 Ga. Among the metasupracrustal rocks is a series of Fe-rich metasedimentary rocks that are of typical quartz + magnetite iron formation, with bulk compositions of 47–61 wt% SiO_2, 20–40 wt% FeO, and 1–3 wt% Al_2O_3 (Mueller et al., 1985). The iron formations are massive to banded with respect to modal amounts of the constituent minerals. The most commonly developed assemblage is quartz + magnetite + ferrosilite + almandine + clinopyroxene. Blue-green amphibole and dark brown biotite are found in trace to minor amounts. Apatite is ubiquitous but only in trace amounts. Applications of various geothermobarometers yield peak metamorphic temperatures and pressures in the ranges of 750–800 °C and 5–6 kbar (Henry, 1990). Subsequent amphibolite-facies metamorphism reset some adjacent lithologies but did not significantly affect the iron formations except near late fractures (Henry and Sella, 1993).

A massive silicate-rich iron formation sample (QC82-45) was chosen for this study because it contains relatively abundant biotite and amphibole. Description of the sample and mineral chemical data have been reported by Henry (1990). The granulite-facies mineral assemblage in this sample is quartz + magnetite + ilmenite + ferrosilite + garnet + biotite + calcic amphibole + zircon ± plagioclase ± apatite. All the major minerals are in mutual contact. Biotite and amphibole are unevenly distributed in the sample and are found as both matrix minerals and inclusions in orthopyroxene and garnet. Localized lower amphibolite-facies retrogressive alteration is developed along fractures cutting through the sample.

Mineral descriptions

Biotite

Dark-brown biotite was interpreted by Henry (1990) as a product of prograde metamorphism of the iron formations. Electron microprobe analyses (Henry, 1990) indicate that this biotite is very Fe-rich (about 80% annite with respect to the annite-phlogopite binary) and contains high Cl, Ba, and Ti concentrations (up to 2.9 wt% Cl, 10.5 wt% BaO, and 6.9 wt% TiO_2, respectively). We refer to this biotite as primary biotite, to distinguish it from the more Fe-rich biotite that apparently formed later as submicrometer inclusions in amphibole, which we refer to as late annite.

Calcic amphibole

Blue-green calcic amphibole (Fig. 1A) was interpreted by Henry (1990) as a preserved prograde metamorphic product. Electron microprobe analyses by Henry (1990) show that the amphibole compositions fall in the field of hastingsite (nomenclature scheme of Leake, 1978). Cl concentrations are very high, up to 2.8 wt%.

Retrograde amphibole

Yellow to greenish grunerite occurs as an alteration product of orthopyroxene along its grain boundaries or in veins passing through orthopyroxene crystals (Fig. 1B). Fracture-related grunerite is associated with ankerite, magnesiosiderite, and clinopyroxene. Henry (1990) and

Henry and Sella (1993) interpreted the grunerite as a product of retrograde, lower amphibolite-facies metamorphism. Electron microprobe analyses show that this amphibole contains much less Cl than the prograde hastingsite (Henry, unpublished data).

Transmission electron microscopy

Sample preparation and experimental techniques

Detailed descriptions of the TEM instrument and experimental methods are given by Veblen and Bish (1988) and Livi and Veblen (1987). A brief discussion of experimental techniques and sample preparation is given here.

Rock samples were made into thin sections, which were mounted with a heat-sensitive cement (Crystalbond 509). Cu grids were glued with epoxy to biotite and amphibole grains in the thin section. The grids were removed from the glass slides, and the specimens were Ar-ion milled to electron transparency. The thin specimens were lightly coated with C to render them conductive in the electron beam. Observations were made at the thin edges of these samples, which occur around perforations in the sections.

TEM was performed at the Johns Hopkins University with a Philips 420ST transmission electron microscope operated at 120 keV. Biotite and amphibole grains were characterized by SAED, conventional TEM, HRTEM, and X-ray emission AEM. The line resolution of the instrument is 0.14 nm. Spatial resolution of the compositional analyses (90% column) varies as a function of specimen geometry and material analyzed but is a minimum of ~20 nm under ideal circumstances. X-ray spectra were collected with an EDAX Li-drifted, solid-state, energy-dispersive detector. Analyses were obtained in a conventional TEM mode, with spot sizes ranging from approximately 20 to 100 nm in diameter. Analyses were quantified using a thin-film ratio method and experimentally determined k factors. Details concerning quantitative analysis are given in Livi and Veblen (1987). Synthetic KCl was used as the Cl standard. A low beam intensity was chosen to prevent beam damage for both the standard and the mineral during data collection. The accuracy of analyses for most major elements is estimated to be about 5%. For K, errors may be higher from possible alkali loss from the analysis spot. The detection limit for most elements is 0.1–0.2 wt%.

Because the biotite and amphibole are Fe-rich, appreciable absorption of X-rays from Al, Mg, Si, and Cl occurred. As a result, the analytical totals for elements lighter than Fe, including Cl, are slightly lower than those from microprobe analyses obtained by Henry (1990). To minimize this effect, an effort was made to analyze areas as close to the thin edge as possible. This was accomplished by working at high magnification and by elongating the beam parallel to the edge of the specimen with the condenser lens stigmator controls.

Experimental results

Primary biotite. Figure 2 shows a HRTEM image of Cl-rich biotite and a SAED pattern from the area shown in the image. The HRTEM image indicates that this Cl-rich biotite is free of inclusions or alteration products such as other intergrown sheet silicates. SAED patterns indicate that the biotite occurs in $1M$, $1M_d$, and also in nine-layer and ten-layer polytypes.

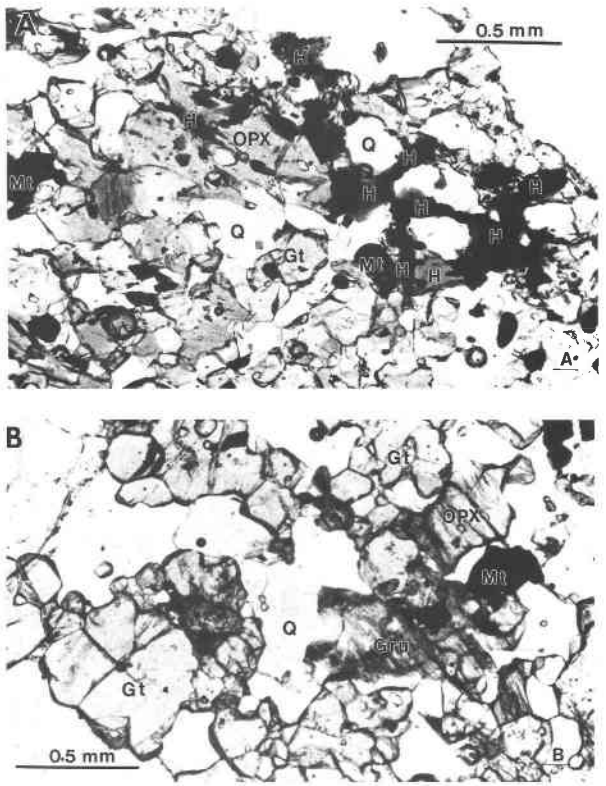

Fig. 1. Photomicrographs showing (**A**) primary hastingsite and (**B**) retrograde grunerite from the alteration of pyroxene along the edges of grains. Mineral abbreviations: OPX = orthopyroxene, Gru = grunerite, Mt = magnetite, Gt = garnet, Q = quartz, H = hastingsite.

AEM analyses of pure biotite, such as those shown in Figure 2, indicate high Cl concentrations (up to 2.8 wt%: Table 1). The Cl distribution within a grain is fairly homogeneous, and the 0.5 wt% variation from grain to grain may result from the Mg-Cl avoidance rule (Munoz, 1984). Figure 3A shows the AEM data for Cl plotted against Mg content. Although the data suggest a negative correlation between Cl and Mg, there is much scatter. Cl and Mg concentrations are lower than those from microprobe analyses (Henry, unpublished data), probably due to the aforementioned X-ray absorption and because F was not included in AEM analyses. The latter contributes to lower calculated $\log(X_{Cl}/X_{OH})$ values because of the assumption $X_{Cl} + X_F + X_{OH} = 1.0$ used in the data reduction. More precise electron microprobe analyses (Fig. 3B), however, show that Cl concentration variation is consistent with the reciprocal interaction model of Zhu and Sverjensky (1992). Taken together, the SAED, HRTEM, and AEM evidence is consistent with the direct substitution of Cl^-

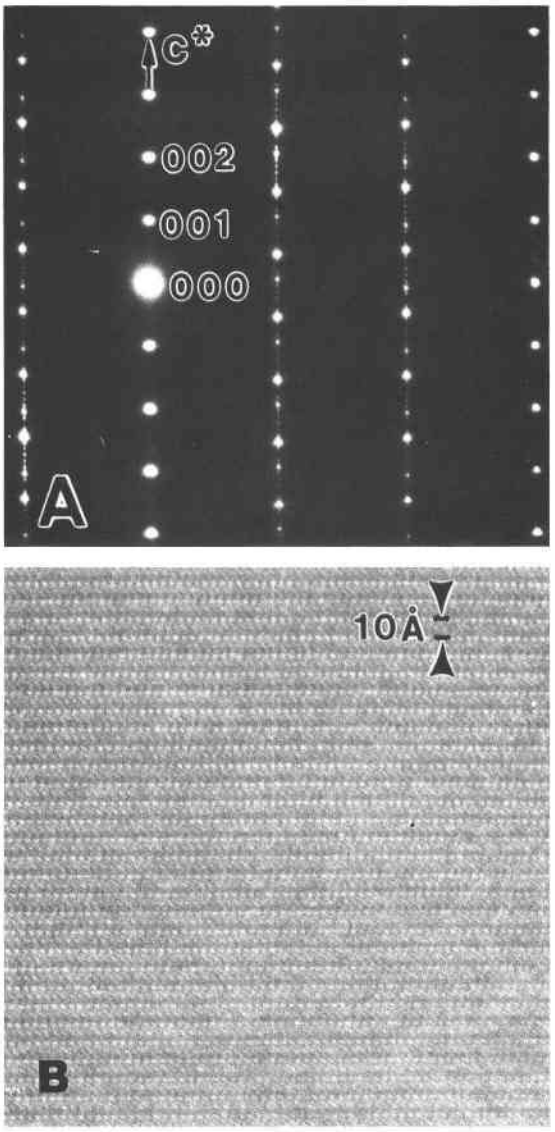

Fig. 2. SAED pattern (A) and HRTEM image (B) of primary, homogeneous, Cl-rich biotite. Together with AEM analyses with up to 2.8 wt% Cl, they indicate that Cl is in solid solution. Note that the lower left portion of the SAED pattern contains reflections indicating a ten-layer biotite polytype.

for structural OH^-, indicating that true Cl-OH solid solution occurs in biotite. This conclusion is further supported by single-crystal X-ray diffraction studies on biotite from the same samples as in this study (Swope et al., 1991; James Munoz, 1993 personal communication).

Biotite examined in this study also has high BaO and TiO_2 concentrations, up to 11 and 5 wt%, respectively. These measured concentrations are comparable to the electron microprobe analyses of Henry (1990, and unpublished data).

Primary Cl-rich calcic amphibole. Several grains of primary hastingsite were chosen for TEM study. An HRTEM image and SAED pattern of Cl-rich hastingsite are shown in Figure 4. The image and sharp diffraction spots show that the hastingsite has homogeneous crystal structure. AEM analyses of such areas indicate high Cl concentrations (Table 1). Consequently, the TEM-AEM evidence is consistent with Cl^- substituting for OH^- in the hastingsite structure, rather than Cl in a separate phase.

Retrograde amphibole. HRTEM images and SAED patterns show that the apparent retrograde amphibole consists of complex intergrowths at the TEM scale. Amphibole of grunerite composition is intergrown with annite, Fe-rich talc,very wide chain pyribole, and Fe-rich clinojimthompsonite domains with sizes from a few to dozens of unit cells along the **b** axis (Figs. 5 and 6). SAED patterns of the annite and talc domains (Fig. 5B, 5C) indicate that the crystals have disordered stacking. AEM analyses (Table 2) show that Cl is contained in annite (1.7–2.8 wt%), Fe-rich talc (~1.0 wt%), and very wide chain pyribole (~0.6 wt%). However, Cl in the grunerite, ferro-clinojimthompsonite, and chain-width disordered areas is below the AEM detection limit (0.1–0.2 wt%). In contrast to the primary amphibole, the late amphibole contains no detectable Ca or K but is also rich in Fe. The submicroscopic annite shows homogeneous Cl distribution. Although Cl concentrations in the retrograde annite (up to 2.8 wt%) are as high as those in the primary, high-temperature annite, the BaO and TiO_2 concentrations are much lower (<2 and <1 wt%).

Petrologic implications for submicrometer-sized inclusions in retrograde amphibole

The most striking feature of Cl concentrations of amphibole reported in the literature is the large variation from grain to grain at a thin section scale (Vanko, 1986; Morrison, 1991; Stakes et al., 1991; Gillis and Thompson, 1993; Henry, 1990, and unpublished data). The above-mentioned amphibole analyses represent samples from a variety of geological environments. Typically, electron microprobe analyses show that some grains contain several thousand parts per million of Cl, but, in others, Cl is below the analytical detection limit (typically about 200 ppm). Crystal chemical control or reciprocal interaction is often cited to explain this variation (e.g., Ito and Anderson, 1983). However, some very sharp variations, such as Cl values from barely detectable up to 4 wt% (Vanko, 1986), are difficult to explain by crystal chemical control alone.

TEM-AEM observations in this study suggest that apparent Cl variations in amphibole can be caused by the submicroscopic intergrowth of Cl-rich sheet silicates. The Cl-rich annite and Fe-rich talc domains intergrown with grunerite in our sample have different sizes, but typically they are less than a few micrometers across. (Note that the field of view is about 0.3 μm in Fig. 5.) Typical electron beam diameters used in electron microprobe analyses of amphibole are 2–10 μm. Therefore, microprobe analyses from different areas of an amphibole grain or

TABLE 1. Representative AEM analyses of hastingsite and primary biotite

Mineral	SiO_2	Al_2O_3	MgO	TiO_2	MnO	FeO*	CaO	Na_2O	K_2O	BaO	Cl
Biotite	28.67	12.69	1.64	4.33	0.14	32.19	1.11	0.00	5.47	11.02	2.24
Biotite	26.93	12.63	1.81	4.17	0.33	34.35	2.35	0.00	4.47	10.49	2.02
Biotite	28.13	12.74	0.94	4.68	0.22	34.85	1.06	0.00	4.80	9.99	2.10
Biotite	28.19	13.28	2.46	4.57	0.16	33.55	0.68	0.00	5.07	9.18	2.35
Atomic proportions based on total +22 cation charges and the assumption of Fe^{2+}											
	Si^{4+}	Al^{3+}	Mg^{2+}	Ti^{4+}	Mn^{2+}	Fe^{2+}	Ca^{2+}	Na^{+}	K^{+}	Ba^{2+}	Cl^{-}
Biotite	2.45	1.28	0.21	0.28	0.01	2.30	0.10	0.00	0.61	0.38	0.33
Biotite	2.32	1.29	0.24	0.27	0.02	2.48	0.22	0.00	0.50	0.36	0.36
Biotite	2.41	1.29	0.12	0.31	0.02	2.50	0.10	0.00	0.53	0.34	0.31
Biotite	2.37	1.32	0.31	0.30	0.01	2.37	0.06	0.00	0.56	0.31	0.34
	SiO_2	Al_2O_3	MgO	TiO_2	MnO	FeO*	CaO	Na_2O	K_2O	BaO	Cl
Hastingsite	38.83	10.91	4.23	1.49	0.30	28.85	11.06	0.13	2.49	—	1.40
Hastingsite	39.42	11.79	3.51	1.76	0.17	28.18	10.66	0.00	2.60	—	1.56
Hastingsite	37.73	12.48	4.42	1.91	0.27	28.03	10.42	0.91	2.23	—	1.31
Hastingsite	40.35	12.45	3.20	1.41	0.03	24.97	11.74	0.00	3.06	—	2.29
Atomic proportions based on total +46 cation charges and the assumption of Fe^{2+}											
	Si^{4+}	Al^{3+}	Mg^{2+}	Ti^{4+}	Mn^{2+}	Fe^{2+}	Ca^{2+}	Na^{+}	K^{+}	Ba^{2+}	Cl^{-}
Hastingsite	6.12	2.03	0.99	0.18	0.04	3.81	1.86	0.04	0.50	—	0.38
Hastingsite	6.16	2.17	0.82	0.21	0.02	3.69	1.78	0.00	0.52	—	0.42
Hastingsite	5.93	2.31	1.03	0.23	0.04	3.68	1.75	0.28	0.45	—	0.35
Hastingsite	6.17	2.25	0.73	0.17	0.00	3.23	1.93	0.00	0.61	—	0.61

* Fe is assumed to be Fe^{2+}.

different grains in a thin section give heterogeneous Cl concentrations as they sample varying amounts of sheet silicates. Furthermore, the analyses could show apparent correlations between Cl and K, Si, and Al concentrations (Fig. 7). We speculate that some reported large Cl variations in electron microprobe analyses may result from submicrometer intergrowths of amphibole with high-Cl phases such as those found in this study. Clearly, caution must be exercised when interpreting microprobe analyses showing Cl variation. We suggest that more TEM-AEM work to examine the reported heterogeneity and correlations must be done before we can interpret them with confidence. In particular, TEM-AEM study is certainly necessary to understand complex amphibole from hydrothermally altered gabbros in midocean ridge systems.

The warning of potentially fortuitous correlations does not mean that compositional correlations resulting from reciprocal interactions between ions on neighboring sites are not important for amphibole. In fact, many studies suggest likely reciprocal effects between Mg-Fe ratios, A-site occupancy, and Cl concentrations (Volfinger et al., 1985; Morrison, 1991; Oberti et al., 1993). However, we emphasize the difficulties in establishing them and especially in quantifying them. In addition to artifacts resulting from solid inclusions, factors like different compositions and pH of fluids that reacted with amphibole and different temperatures and pressures of reactions can also result in apparent correlation or apparent scatter in compositions for amphibole from different rocks. The latter factors were demonstrated for biotite by Zhu and Sverjensky (1992).

PETROLOGIC INTERPRETATION OF Cl ENRICHMENT IN PRIMARY AMPHIBOLE AND BIOTITE

Causes of Cl enrichment

The Cl-OH substitution in biotite and amphibole is a function of temperature, pressure, fluid composition, and crystal chemistry (Munoz, 1984; Volfinger et al., 1985; Zhu and Sverjensky, 1991, 1992). Thermodynamic calculations indicate that high temperatures facilitate Cl^- substitution for OH^- in biotite (see Appendix 1).

The primary biotite in this study contains BaO and TiO_2 concentrations of 11 and 5 wt%, respectively, and Ba occupies up to about 35% of the interlayer sites (Table 1 for AEM analyses and Henry, 1990, for electron microprobe analyses). Henry (1990, and unpublished data) also found that Ba concentrations positively correlate with Cl concentrations in biotite. In addition, Tracy (1991) reported that Ba-rich biotite (up to 23 wt% BaO) from the Sterling Hill skarn, New Jersey, contains up to 7.15 wt% Cl, and this occurrence shows similar Ba-Cl positive correlations. Such correlations may lead to the suspicion that high Cl concentrations are related to high Ba and Ti concentrations and resulting structural changes in biotite and amphibole. However, we would argue that Cl enrichment in biotite and amphibole is mainly due to a Cl-rich environment, perhaps caused by reactions with a saline brine (see below), on the basis of the following lines of evidence. First, AEM analyses of retrograde annite intergrown with grunerite show little Ba or Ti, but they indicate Cl concentrations as high as those of the high-Ba, high-Ti primary annite samples. Second, apatite in the

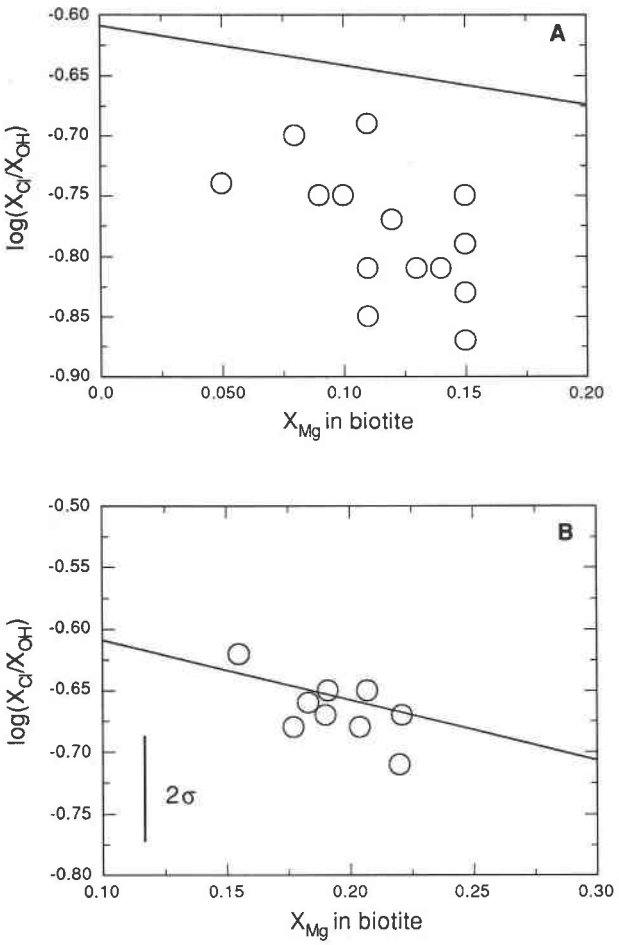

Fig. 3. Plots of (**A**) AEM analyses of primary biotite and (**B**) electron microprobe analyses of biotite matrix. Grain to grain Cl variation is consistent with the Mg-Cl avoidance rule (Munoz, 1984). The lines on both graphs have a slope of −0.5, which was calculated independently from the reciprocal solution model of Zhu and Sverjensky (1992). The intercept was visually fitted to pass the data on **B**. The vertical bar represents 2 sd, resulting from a 4% analytical uncertainty in Cl electron microprobe analyses (Henry, unpublished data). Note the large scale on the y axis; the scales are the same for both plots.

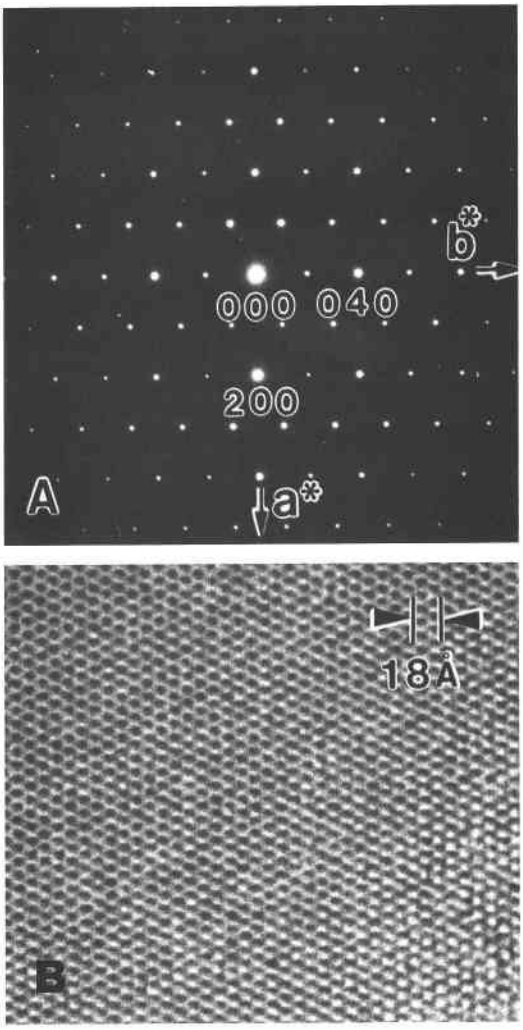

Fig. 4. SAED pattern (**A**) and HRTEM image (**B**) of primary Cl-rich hastingsite, showing homogeneous structure. AEM results of this area indicate up to 2.3 wt% Cl. Together, they indicate that Cl is in the crystal structure. Most notable is the absence of any biopyribole alteration (e.g., chain-width disorder and sheet silicate slabs).

samples also shows high Cl concentrations (see Appendix 2), and geochemical modeling using the apatite halogen concentrations suggests the possible equilibrium reaction with a saline brine (see below). The apatite halogen compositions are used because the approximation of the activity-composition relationship needed for modeling is better constrained for apatite than those for Ba- and Ti-rich biotite or hastingsite.

Modeling fluid compositions

We can use the halogen concentrations of apatite (Appendix 2) to calculate the activity ratio, a_{HCl^0}/a_{H_2O}, in the fluids that were at equilibrium with the apatite from the reaction

$$\underset{\text{hydroxylapatite}}{Ca_5(PO_4)_3(OH)} + HCl^0 = \underset{\text{chlorapatite}}{Ca_5(PO_4)_3(Cl)} + H_2O. \quad (1)$$

If one assumes ideal mixing of Cl-F-OH in apatite, an expression of the law of mass action is given by

$$\log K_1 = \log\left(\frac{X_{Cl}}{X_{OH}}\right) - \log\left(\frac{a_{HCl^0}}{a_{H_2O}}\right) \quad (2)$$

where K_1 represents the equilibrium constant of Reaction 1, X_{Cl} and X_{OH} denote the mole fractions of Cl and OH in apatite, and a_{HCl^0} and a_{H_2O} stand for activities of HCl^0 and H_2O, respectively. The standard states for hydroxylapatite and chlorapatite are pure end-member components at the temperature and pressure of interest. The standard states for aqueous species other than H_2O are

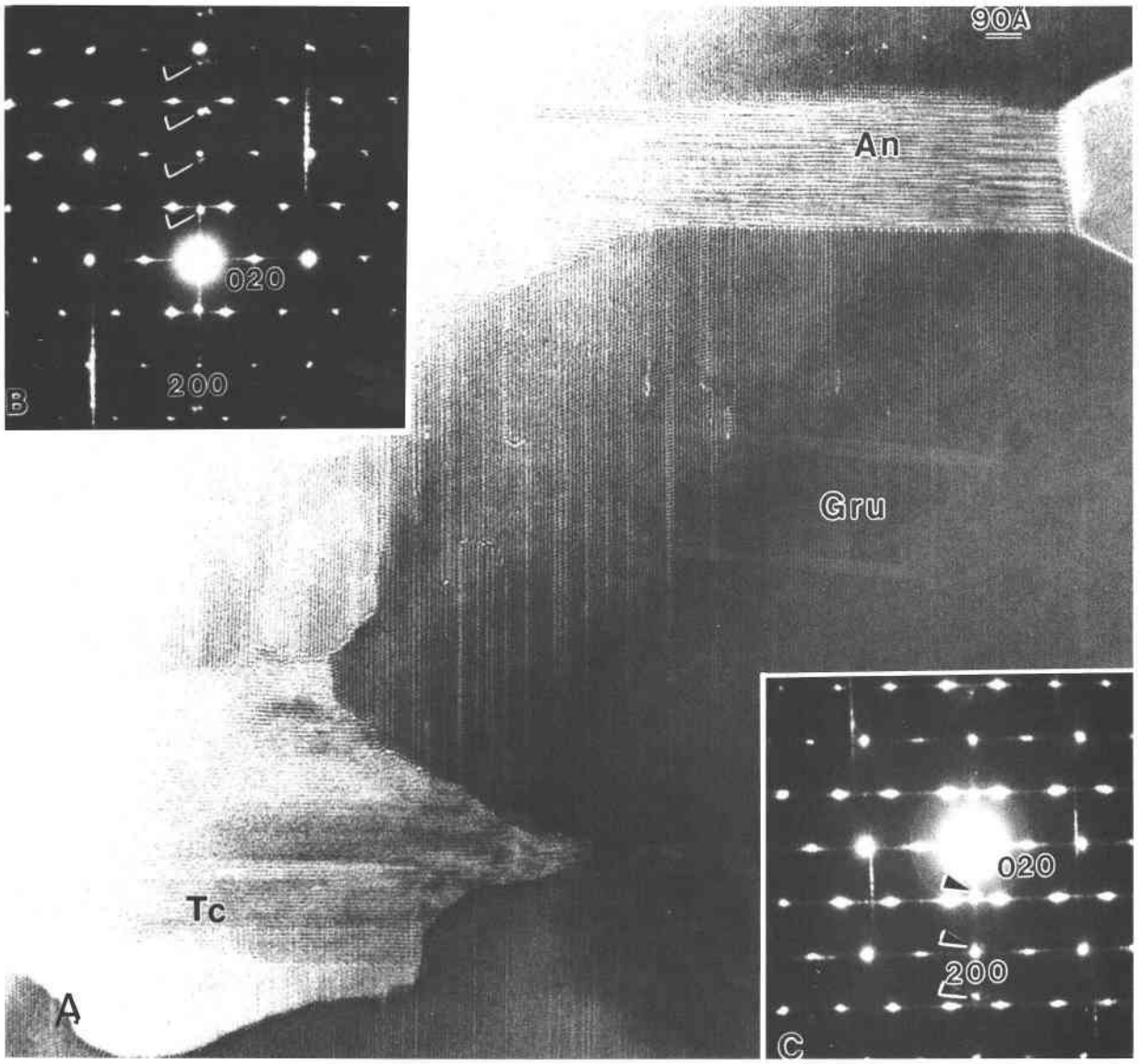

Fig. 5. An HRTEM image (A) of Cl-bearing grunerite, showing chain-width disorder, an annite domain (An), and an Fe-rich talc domain (Tc) within the crystal. SAED patterns include scattering from the annite domain (B) and Fe-rich talc domain (C). Arrows indicate 00*l* sheet silicate diffraction. AEM analyses indicate that these submicrometer-sized annite domains contain as much as 2.8 wt% Cl.

hypothetical, 1-*m* ideal solutions at the temperature and pressure of interest, and, for H_2O, the standard state is unit activity of pure H_2O at the P and T of interest.

The value of log K_1 at 750 °C and 6 kbar is calculated to be 1.83 using the data and method of Zhu and Sverjensky (1992). Values of $\log(a_{HCl^0}/a_{H_2O})$ are then calculated to be -1.8 to -2.2 using the composition data in Appendix Table 1.

It is instructive to evaluate the Cl^- concentrations of an aqueous fluid that would have been in equilibrium with the high-Cl apatite, biotite, and primary amphibole in our samples. Speciation and solubility calculations were carried out to simulate the compositions of aqueous fluids that would be in equilibrium with the mineral assemblage quartz + ferrosilite + garnet + biotite + plagioclase + apatite. The calculated a_{HCl^0}/a_{H_2O} ratios from the apatite Cl-OH exchange reaction were used to constrain the Cl concentration of the aqueous phase. By so doing, we are assuming that the apatite was in equilibrium with the biotite and amphibole (see Appendix 2). The method and sources of thermodynamic data are described by Zhu and Sverjensky (1991, 1992) and Zhu (1993). The activity for H_2O was assumed to be unity, as possible CO_2 contents in the aqueous phases were neglected. Activity coefficients for ionic species were calculated following the method of Helgeson et al. (1981). Activities for mineral

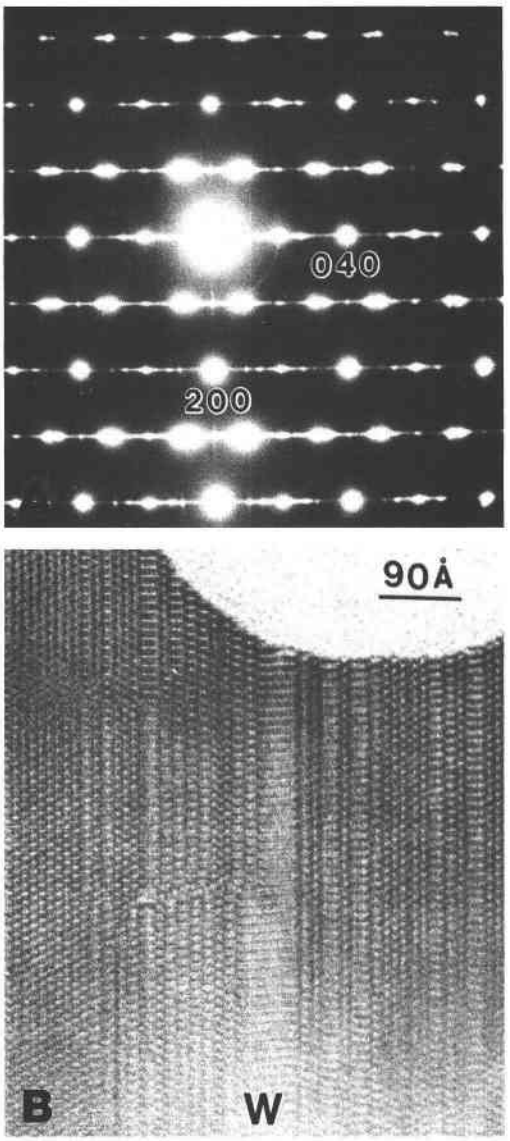

Fig. 6. SAED pattern (**A**) and HRTEM image (**B**) showing chain-width disordered grunerite and a very wide chain pyribole (W) that also contains Cl.

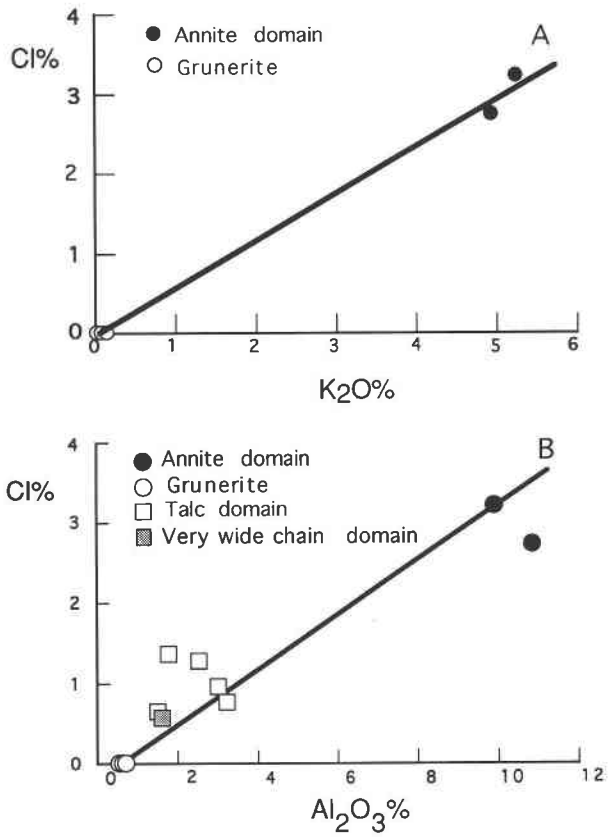

Fig. 7. Plots of AEM analyses of annite, grunerite, and talc domains in grunerite, showing schematically that fortuitous correlations could be a result of probing different proportions of these domains. (**A**) Cl vs. K_2O; (**B**) Cl vs. Al_2O_3 (wt%).

components were calculated using electron microprobe analyses from Henry (unpublished data) and the solid solution models for garnet (Berman, 1990), for orthopyroxene (Sack and Ghiorso, 1989), for biotite (Zhu and Sverjensky, 1992), and for plagioclase (Ghiorso, 1984). The modeling estimated the total dissolved Cl^- concentrations in the hypothesized aqueous phase to be about 4 *m* (Table 3), or about 25 wt% NaCl, with the assumption that the fluid was in equilibrium with the Cl-rich biotite, amphibole, apatite, and the above-mentioned mineral assemblage.

The calculated salinity of the hypothesized aqueous fluid at local equilibrium with the Cl-rich apatite, biotite, and primary amphibole in our samples is only a first approximation and perhaps represents a conservative estimate. Dissolved CO_2 and CH_4 in H_2O would reduce the dielectric constant of H_2O, which would increase the activities of uncharged species (Walther, 1991). A decrease in the activity of H_2O and an increase in the activity of HCl^0 would promote Cl-OH substitution in biotite, amphibole, and apatite (cf. Eq. 2).

Discussion of possible petrologic implications

The Cl content of apatite and the above calculations imply that a brine with ~25 wt% equivalent NaCl (relative to H_2O) at approximately 750 °C and 6 kbar could be associated with the formation of the primary Cl-rich minerals in our granulite sample. High-CO_2 fluid inclusions and low calculated H_2O activities are also found in this sample (Henry, 1990). However, both lines of evidence are consistent with the hypothesis that there were actually coexisting immiscible fluids during the granulite-facies metamorphism: a saline brine and a CO_2-dominant vapor. The hypothesis of coexisting, immiscible, brine + CO_2 fluids has long been regarded as a strong possibility (Bowers and Helgeson, 1983; Trommsdorff and Skippen, 1986, 1987; Thompson, 1987; Yardley and Bottrell, 1988; Crawford and Hollister, 1986; Johnson, 1991; Frantz et

TABLE 2. Representative AEM analyses of later retrograde grunerite, annite, talc, and wide-chain silicate

Mineral	SiO_2	Al_2O_3	MgO	TiO_2	MnO	FeO*	CaO	Na_2O	K_2O	BaO	Cl
Grunerite	52.32	0.62	9.83	0.01	1.01	35.78	0.13	0.21	0.00	—	
Grunerite	51.67	0.61	11.13	0.02	1.00	35.31	0.18	0.16	0.05	—	
Grunerite	51.14	0.61	9.78	0.03	1.12	36.87	0.25	0.09	0.11	—	
Atomic proportions based on total +46 cation charges and the assumption of Fe^{2+}											
	Si^{4+}	Al^{3+}	Mg^{2+}	Ti^{4+}	Mn^{2+}	Fe^{2+}	Ca^{2+}	Na^{+}	K^{+}	Ba^{2+}	Cl^{-}
Grunerite	7.94	0.11	2.22	0.01	0.13	4.53	0.02	0.06	0.00	—	
Grunerite	7.89	0.11	2.53	0.02	0.13	4.50	0.03	0.05	0.01	—	
Grunerite	7.83	0.11	2.22	0.02	0.13	4.71	0.04	0.03	0.02	—	
	SiO_2	Al_2O_3	MgO	TiO_2	MnO	FeO*	CaO	Na_2O	K_2O	BaO	Cl
Annite	35.47	10.91	5.76	0.82	0.36	36.14	0.00	1.04	4.88	1.89	1.69
Annite	37.68	9.44	2.55	0.83	0.15	39.01	0.00	0.00	5.24	1.86	1.66
Wide chain	49.21	1.51	11.32	0.03	0.05	34.58	0.22	1.18	0.45	0.01	0.57
Talc	47.39	2.55	7.03	0.00	0.60	39.13	0.06	1.35	0.53	0.00	1.10
Talc	47.22	1.85	6.90	0.19	0.58	39.33	0.00	1.76	0.38	0.00	1.17
Talc	46.88	3.03	9.33	0.12	0.05	36.06	0.01	1.22	1.00	0.50	0.77
Atomic proportions based on total +22 cation charges and the assumption of Fe^{2+}											
	Si^{4+}	Al^{3+}	Mg^{2+}	Ti^{4+}	Mn^{2+}	Fe^{2+}	Ca^{2+}	Na^{+}	K^{+}	Ba^{2+}	Cl^{-}
Annite	2.80	1.02	0.68	0.05	0.02	2.40	0.10	0.16	0.50	0.06	0.30
Annite	2.99	0.90	0.31	0.05	0.01	2.60	0.00	0.00	0.54	0.06	0.36
Wide chain	3.60	0.13	1.24	0.00	0.05	2.12	0.02	0.017	0.04	0.00	0.07
Talc	3.57	0.23	0.79	0.00	0.04	2.46	0.00	0.20	0.05	0.00	0.14
Talc	3.57	0.16	0.78	0.01	0.04	2.48	0.00	0.26	0.04	0.00	0.15
Talc	3.50	0.27	1.04	0.01	0.05	2.25	0.01	0.18	0.10	0.01	0.10

* Fe is assumed to be Fe^{2+}.

al., 1992; Joyce and Holloway, 1993). Evidence from both fluid inclusions and phase equilibrium experiments supports this hypothesis. Sisson et al. (1981) found natural fluid inclusions in quartz pods of metamorphic calcareous rocks, indicating the existence of an immiscible brine at conditions of 6.5 kbar, 600 °C, and 24 wt% NaCl, which are similar to those of this study. Johnson (1991) and Joyce and Holloway (1993) conducted experiments in the NaCl-CO_2-H_2O system and found a wide region of immiscibility existing at high-grade metamorphic conditions. Frantz et al. (1992) conducted experimental studies with synthetic fluid inclusions and mass spectrometry at temperatures and pressures of 500–700 °C and 1–3 kbar, and they found that miscibility gaps exist over a wide range of P-T-composition conditions.

Although no experimental data are available for the particular T, P, and bulk fluid composition conditions pertinent to our sample, extrapolation from the observed P, T, and compositional trends indicates that fluids in equilibrium with the high-Cl minerals in this study would likely fall within the immiscibility field. Therefore, results from chemical thermodynamic considerations are consistent with the possible presence of a saline brine coexisting with a CO_2-dominant vapor. The presence of such saline brines would have profound implications for the nature of metamorphic reactions and mass transfer in such environments.

TABLE 3. Constraints and representative results of speciation and solubility calculations

Activities used for mineral end-member components			
Mineral solid solution		Components	Log activities used
Garnet		pyrope	−3.6
Biotite		phlogopite	−2.4
		annite	−0.6
Orthopyroxene		ferrosilite	−0.14
Plagioclase		anorthite	−0.22
		albite	−0.16
		Results	
log a_{HCl^0}	−2.00	pH	4.6
m_{t,Cl^-}	4	Cl^- (%)	40
$NaCl^0$ (%)	38	KCl^0 (%)	21
$CaCl_2^0$ (%)	1	log a_{HF^0}	−1.78
F (ppm)	332	m_{t,F^-}	0.06
HF^0 (%)	98	F^- (%)	2

Note: the mineral assemblage is as follows: quartz + orthopyroxene + garnet + biotite + plagioclase. T = 750 °C; P = 6 kbar. See text for sources of thermodynamic properties for mineral and aqueous species. Mineral compositional data are from Henry (unpublished data).

ACKNOWLEDGMENTS

We thank Greg Anderson for his review of the manuscript, John Frantz for stimulating discussions on fluid immiscibility, Michael Jercinovic and Michael Wise for making and providing apatite microprobe standards, and Larry Ball, Dave DuBois, and Monica Driscoll for generously making their computer facility available to us. Reviews by Jim Munoz, Eugene Smelik, and George Guthrie helped to improve this paper. C.Z. was supported by a postdoctoral fellowship awarded by the Woods Hole Oceanographic Institution. Electron microscopy was supported by NSF grants EAR-8903630 and EAR-8300365 to D.V.

REFERENCES CITED

Bence, A.E., and Albee, A.L. (1968) Empirical correction factors for the electron microprobe analysis of silicates and oxides. Journal of Geology, 76, 382–403.

Berman, R.G. (1990) Mixing properties of Ca-Mg-Fe-Mn garnets. American Mineralogist, 75, 328–344.

Blattner, P. (1980) Chlorine-enriched Leucogabbro in Nelson and Fiorland, New Zealand. Contributions to Mineralogy and Petrology, 2, 486–490.

Bowers, T.S., and Helgeson, H.C. (1983) Calculation of the thermodynamic and geochemical consequences of nonideal mixing in the system H_2O-CO_2-NaCl on the phase relations in geological systems: Equation of state for H_2O-CO_2-NaCl fluids at high pressures and temperatures. Geochimica et Cosmochimica Acta, 47, 1247–1275.

Brehler, B., and Fuge, R. (1974) Chlorine. In K.H. Wederpohl, Ed., Handbook of geochemistry, vol. 2 (4), chapter 17, p. 1–36. Springer-Verlag, Berlin.

Crawford, M.L., and Hollister, L.S. (1986) Metamorphic fluids: The evidence from fluid inclusions. In J.V. Walther and B.J. Wood, Eds., Fluid-rock interactions during metamorphism, p. 1–36. Springer-Verlag, New York.

Deer, W.A., Howie, R.A., and Zussman, J. (1966) An introduction to the rock-forming minerals, 528 p. Longmans, New York.

Dick, L.A., and Robinson, G.W. (1979) Chlorine-bearing potassium hastingsite from a sphalerite skarn in southern Yukon. Canadian Mineralogist, 17, 25–26.

Donnay, G., Shaw, C.F., III, Butler, I.S., and O'Neil, J.R. (1978) The presence of HCl in scapolites. Canadian Mineralogist, 16, 341–345.

Frantz, J.D., Popp, R.K., and Hoering, T.C. (1992) The compositional limits of fluid immiscibility in the system H_2O-NaCl-CO_2 as determined with the use of synthetic fluid inclusions in conjunction with mass spectrometry. Chemical Geology, 98, 237–255.

Ghiorso, M.S. (1984) Activity/composition relations in the ternary feldspars. Contributions to Mineralogy and Petrology, 87, 282–296.

Gillis, K.M., and Thompson, G. (1993) Metabasalts from the mid-atlantic ridge: New insights into hydrothermal systems in slow-spreading crust. Contributions to Mineralogy and Petrology, 113, 502–523.

Gulyaeva, T.Ya., Gorelikova, N.V., and Karabtsov, A.A. (1986) High potassium-chlorine-bearing hastingsites in skarns from Primorye, far east USSR. Mineralogical Magazine, 50, 723–728.

Helgeson, H.C., Kirkham, D.H., and Flowers, G.C. (1981) Theoretical prediction of the thermodynamic behavior of aqueous electrolytes at high pressures and temperatures. IV. Calculation of activity coefficients, osmotic coefficients, and apparent molal and standard and relative partial molal properties to 600° C and 5 kbar. American Journal of Science, 281, 1249–1516.

Henry, D.J. (1990) Cl-rich minerals in Archean granulite facies ironstones from Beartooth mountains, Montana, USA: Implications for fluids involved in granulite metamorphism (abs.). Crust of India Symposium, p. 43–45.

Henry, D.J., and Sella, G.A. (1993) Nitrogen fluid inclusions associated with retrograde metamorphism. Geological Society of America Abstracts with Programs, 24 (5), A158.

Henry, D.J., Mueller, P.A., Wooden, J.L., and Lee-Berman, R. (1982) Granulite grade supracrustal assemblages of the Quad Creek area, eastern Beartooth Mountains, Montana. In P.A. Mueller and J.L. Wooden, Eds., Precambrian geology of the Beartooth Mountains, Montana and Wyoming. Montana Bureau of Mines and Geology special publications, 84, p. 147–159.

Ito, E., and Anderson, A.T., Jr. (1983) Submarine metamorphism of gabbros from the Mid-Cayman Rise: Petrographic and mineralogic constraints on hydrothermal processes at slow-spreading ridges. Contributions to Mineralogy and Petrology, 82, 371–388.

Jarosewich, E., Nelen, J.A., and Norberg, J.A. (1980) Reference samples for electron microprobe analysis. Geostandards Newsletter, 4, 43–47.

Johnson, E.L. (1991) Experimentally determined limits for H_2O-CO_2-NaCl immiscibility in granulites. Geology, 19, 925–928.

Joyce, D.B., and Holloway, J.R. (1993) An experimental determination of the thermodynamic properties of H_2O-CO_2-NaCl fluids at high pressures and temperatures. Geochimica et Cosmochimica Acta, 57, 733–746.

Kamineni, D.C., Bonardi, M., and Rao, A.T. (1982) Halogen-bearing minerals from Airport Hill, Visakhapatnam, India. American Mineralogist, 67, 1001–1004.

Leake, B.E. (1978) Nomenclature of amphiboles. Canadian Mineralogist, 16, 501–520.

Livi, K.J.T., and Veblen, D.R. (1987) "Eastonite" from Easton, Pennsylvania: A mixture of phlogopite and a new form of serpentine. American Mineralogist, 72, 113–125.

Mogk, D.W., and Henry, D.J. (1988) Metamorphic petrology of the northern Archean Wyoming Province, SW Montana: Evidence for Archean collisional tectonics. In W.G. Ernst, Ed., Metamorphism and crustal evolution of the western U.S., p. 147–160. Prentice-Hall, Englewood Cliffs, New Jersey.

Morrison, J.M. (1991) Compositional constraints on the incorporation of Cl into amphiboles. American Mineralogist, 76, 1920–1930.

Mueller, P.A., Wooden, J.L., Henry, D.J., Bowes, D.R. (1985) Archean crustal evolution of the eastern Beartooth Mountains, Montana and Wyoming. In G.K. Czamanske and M.L. Zientek, Eds., The Stillwater complex. Montana Bureau of Mines and Geology Special Publication, 92, p. 9–12.

Munoz, J.L. (1984) F-OH and Cl-OH exchange in micas with applications to hydrothermal ore deposits. In Mineralogical Society of America Reviews in Mineralogy, 13, 469–493.

Munoz, J.L., and Swenson, A. (1981) Chloride-hydroxyl exchange in biotite and estimation of relative HCl/HF activities in hydrothermal fluids. Economic Geology, 76, 2212–2221.

Nash, J.T. (1989) Chlorine-rich biotite from Blackbird Mining district, Lemhi, Idaho—Evidence for a saline hydrothermal brine. U.S. Geological Survey Open Report 89-445.

Nash, P.T. (1984) Phosphate minerals in terrestrial igneous and metamorphic rocks. In J.O. Nriagu and P.B. Moore, Eds., Phosphate minerals, p. 215–241. Springer-Verlag, Berlin.

Newberry, N.G., Essene, E.J., and Peacor, D.R. (1981) Alforsite, a new member of the apatite group: The barium analogue of chlorapatite. American Mineralogist, 66, 1050–1053.

Oberti, R., Ungaretti, L., Cannillo, E., and Hawthorne, F.C. (1993) The mechanism of Cl incorporated in amphibole. American Mineralogist, 78, 746–752.

Sack, R.O., and Ghiorso, M.S. (1989) Importance of considerations of mixing properties in establishing an internally consistent thermodynamic database: Thermochemistry of minerals in the system Mg_2SiO_4-Fe_2SiO_4-SiO_2. Contributions to Mineralogy and Petrology, 102, 41–68.

Sisson, V.B., Crawford, M.L., and Thompson, P.H. (1981) CO_2-brine immiscibility at high temperatures, evidence from calcareous metasedimentary rocks. Contributions to Mineralogy and Petrology, 78, 371–378.

Stakes, D.S., Mevel, C., Cannat, M., and Chaput, T. (1991) Metamorphic stratigraphy of hole 735B. In R.P. Von Herzen and P.T. Robinson, Eds., Proceedings of ocean drilling program, vol. 118, Scientific results, p. 153–180. College Station, Texas.

Suwa, K., Enami, M., and Horiuchi, T. (1987) Chlorine-rich potassium hastingsite from west island, Lützow-Holm Bay, East Antarctica. Mineralogical Magazine, 51, 709–714.

Swope, R.J., Smyth, J.R., and Munoz, J.L. (1991) Crystal structure refinement of Cl-rich 1*M* biotite. Geological Society of America Abstracts with Programs, 23 (5), A158.

Symmes, G.H., and Ferry, J.M. (1992) Evidence from mineral assemblages for infiltration of pelitic schists by aqueous fluids during metamorphism. Contributions to Mineralogy and Petrology, 108, 419–438.

Thompson, A.B. (1987) Some aspects of fluid motion in metamorphism. Journal of the Geological Society of London, 144, 309–312.

Tracy, R.J. (1991) Ba-rich micas from the Franklin Marble, Lime Crest and Sterling, New Jersey. American Mineralogist, 76, 1683–1693.

Trommsdorff, V., and Skippen, G. (1986) Vapour loss ("boiling") as a mechanism for fluid evolution in metamorphic rocks. Contributions to Mineralogy and Petrology, 94, 317–322.

——— (1987) Metamorphism involving fluids in CO_2-H_2O-NaCl. In H.C. Helgeson, Ed., Chemical transport in metamorphic processes, p. 133–152. NATO ASI Series C218, Reidel, Dordrecht, The Netherlands.

Tyler, R.D. (1979) Chloride metasomatism in the Southern part of the Pierrepond Quadrangle, Adirondack Mountains, New York. Ph.D. dissertation, State University of New York, Binghamton, New York.

Valley, J.W., Bohlen, S.R., Essene, E.J., and Lamb, W. (1990) Metamorphism in the Adirondacks. II. The role of fluids. Journal of Petrology, 31, 555–596.

Vanko, D.A. (1986) High-chlorine amphiboles from oceanic rocks: Prod-

uct of highly-saline hydrothermal fluids? American Mineralogist, 71, 51–59.

Veblen, D.A., and Bish, D.L. (1988) TEM and X-ray study of orthopyroxene megacryst: Microstructures and crystal chemistry. American Mineralogist, 73, 677–691.

Volfinger, M., Robert, J.L., Vielzeuf, D., and Neiva, A.M.R. (1985) Structural control of the chlorine content of OH-bearing silicates (micas and amphiboles). Geochimica et Cosmochimica Acta, 49, 37–48.

Walther, J.V. (1991) Thermodynamic properties of solutes in H_2O-CO_2-CH_4 and other mixed solvent fluids at elevated temperature and pressure. Geological Society of America Abstracts with Programs, 23 (5), A213.

Yardley, B.W.D., and Bottrell, S.H. (1988) Immiscible fluids in metamorphism: Implications of two-phase flow for reaction history. Geology, 16, 199–202.

Zhu, Chen (1993) New pH sensor for hydrothermal fluids. Geology, 21, 983–986.

Zhu, Chen, and Sverjensky, D.A. (1991) Partitioning of F, Cl, OH between minerals and 8 hydrothermal fluids. Geochimica et Cosmochimica Acta, 55, 1837–1858.

——— (1992) F-Cl-OH partitioning between apatite and biotite. Geochimica et Cosmochimica Acta, 56, 3435–3467.

Manuscript received November 18, 1993
Manuscript accepted May 6, 1994

Appendix Table 1. Representative microprobe analyses (wt%) of apatite and calculated fluid compositions

	1	1σ	2	1σ
P_2O_5	41.43	0.18	42.83	0.31
F	2.54	0.13	1.41	0.23
Cl	1.36	0.08	1.55	0.35
Al_2O_3	0.02	0.02	0.03	0.00
SiO_2	0.18	0.03	0.13	0.04
CaO	55.85	0.23	57.09	0.15
MgO	0.03	0.03	0.02	0.02
FeO	0.40	0.24	0.19	0.01
Total	101.82	0.25	103.25	0.19
Atoms per 12 O atoms (excluding H_2O, F, and Cl)				
P	2.84	0.01	2.86	0.01
F	0.65	0.03	0.35	0.06
Cl	0.19	0.01	0.21	0.05
OH*	0.16		0.44	
Al	0.00	0.00	0.00	0.00
Si	0.01	0.00	0.01	0.00
Ca	4.84	0.02	4.82	0.01
Mg	0.00	0.00	0.00	0.00
Fe	0.03	0.02	0.01	0.00
$\log(a_{HCl}/a_{H_2O})$**	−2.2		−1.8	
$\log(a_{HF^0}/a_{H_2O})$**	−1.8		−2.3	

* OH estimated by difference $X_{OH} = 1 - X_F - X_{Cl}$.
** See text.

Appendix 1. Evaluating Cl and F concentrations of hydrothermal and metamorphic fluids

Early calculations in some model systems demonstrate the *T*, *P*, and fluid-composition dependence of F-Cl-OH partitioning among minerals and hydrothermal fluids (Zhu and Sverjensky, 1991). However, we used annite as a proxy for biotite because we were not able to deal with the influences of Fe-Mg ratios on the partitioning quantitatively. Such results are limited in applications because natural biotite contains variable Fe-Mg ratios. The work of Zhu and Sverjensky (1992) permits quantitatively assessing the reciprocal effects, and, therefore, calculations taking these effects into account are more useful. In addition, the value of Gibbs free energy of formation for Cl end-member annite from Zhu and Sverjensky (1991) was modified in Zhu and Sverjensky (1992). Using these new results, F-Cl-OH partitioning between biotite and hydrothermal fluids has been simulated in the system K_2O-Na_2O-CaO-MgO-Al_2O_3-SiO_2-FeO-HCl-HF-H_2O over a wide range of *T* and *P*. Appendix Figure 1A, 1B show the predicted F and Cl concentrations of fluids, which are in equilibrium with the mineral assemblage muscovite + potassium feldspar + quartz + albite + biotite—a common hydrothermal alteration assemblage. The F and Cl concentrations of fluids are a function of F and Cl concentrations of biotite, as well as Fe-Mg ratios of biotite. Appendix Figure 1C–1E predict Cl concentrations of hydrothermal and metamorphic fluids, which coexist with mineral assemblages of a typical metapelite from biotite to granulite facies (e.g., Symmes and Ferry, 1992). Appendix Figure 1 demonstrates the significance of taking account of the reciprocal effects on evaluating F and Cl concentrations of fluids. With increasing F and Cl concentrations in biotite, these effects become more significant, and the partitioning curves become divergent. Activities for end-member components of mineral solid solutions different from those used for the above calculations would result in slightly different predicted total F and Cl concentrations. This is especially true for K- and Na-bearing components.

Appendix 2. Apatite compositions

In this study, apatite was found in the silicate-rich part of the iron formations as an accessory mineral in the matrix. Apatite grains are typically small (100–200 μm) with subhedral or round shapes. They are seen in contact with garnet, quartz, and pyroxene. The compositions of apatite have been analyzed using an electron microprobe.

Analytical methods

Electron microprobe analyses were carried out on a JEOL 733 Superprobe at the Massachusetts Institute of Technology. The standard operating conditions were 15-keV acceleration potential, 10-nA beam current, and 10-μm beam diameter. F, Cl, and P were counted first, and counting times for F and Cl were 40 s for both standards and samples. Data reduction was accomplished online by a Bence-Albee method (Bence and Albee, 1968). For F and Cl analysis of apatite, a Wilburforce apatite sample (3.67 wt% F) and a scapolite sample (USNM R6600-1, 1.43 wt% Cl) from the Smithsonian Institution (Jarosewich et al., 1980) were used for standards. Corrections for Cl have been applied by calibrating with a Durango apatite sample (USNM 104021, 0.41 wt%) for the same source.

Results

Typical apatite compositions for our sample show high Cl concentrations (Appendix Table 1). The apatite analyses show homogeneous compositions within a grain. Applying the apatite + biotite geothermometer of Zhu and Sverjensky (1992) gives temperatures of 710–810 °C, which are consistent with temperatures derived from other geothermometers (Henry, 1990). This consistency may indicate equilibrium between apatite and biotite in terms of halogen component exchange, although caution must be exercised because of the possible influence of high Ba, Cl, and Ti concentrations on the partitioning.

Ba was not included in the analysis. Although Ba contents in

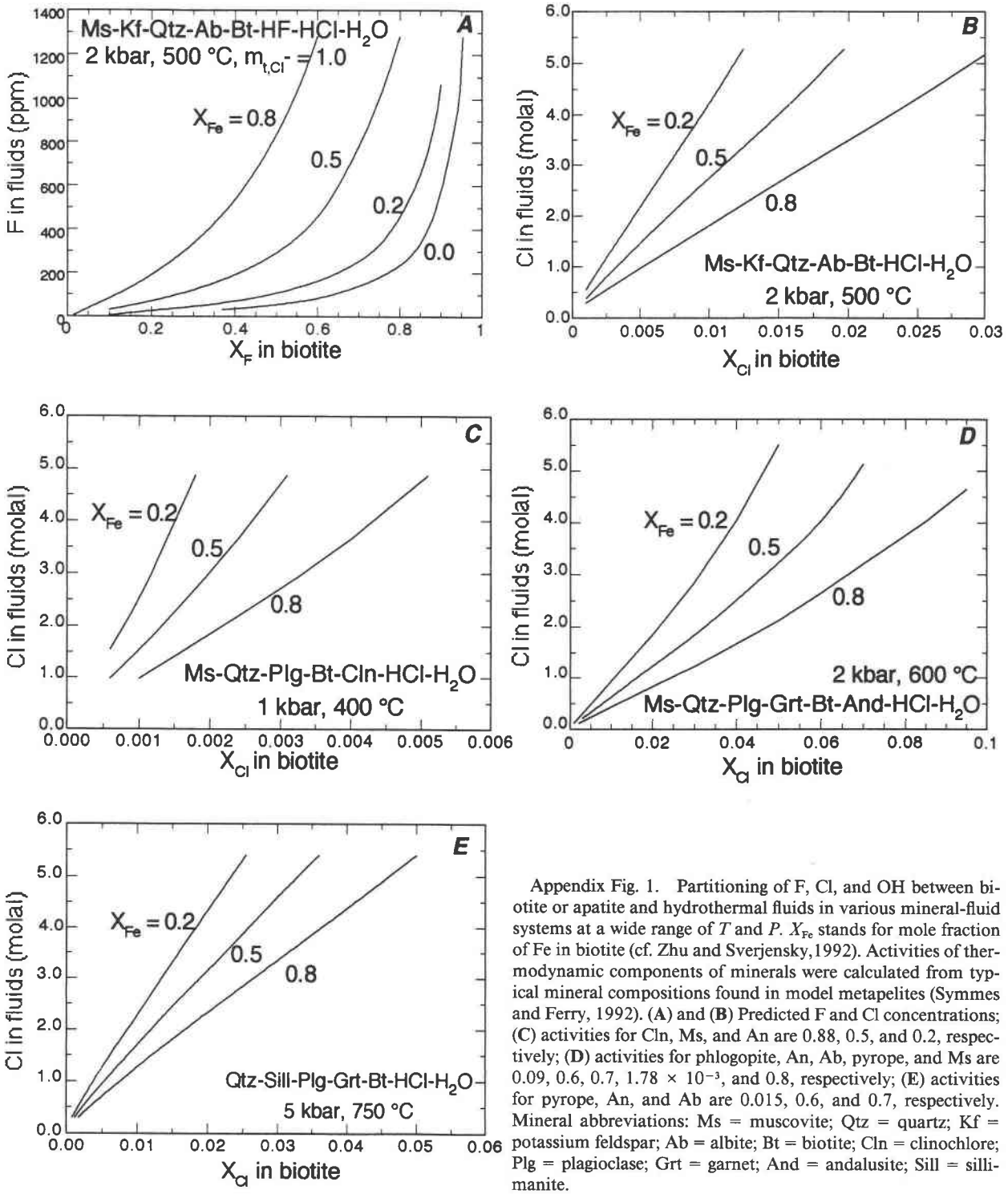

Appendix Fig. 1. Partitioning of F, Cl, and OH between biotite or apatite and hydrothermal fluids in various mineral-fluid systems at a wide range of T and P. X_{Fe} stands for mole fraction of Fe in biotite (cf. Zhu and Sverjensky,1992). Activities of thermodynamic components of minerals were calculated from typical mineral compositions found in model metapelites (Symmes and Ferry, 1992). (**A**) and (**B**) Predicted F and Cl concentrations; (**C**) activities for Cln, Ms, and An are 0.88, 0.5, and 0.2, respectively; (**D**) activities for phlogopite, An, Ab, pyrope, and Ms are 0.09, 0.6, 0.7, 1.78 × 10^{-3}, and 0.8, respectively; (**E**) activities for pyrope, An, and Ab are 0.015, 0.6, and 0.7, respectively. Mineral abbreviations: Ms = muscovite; Qtz = quartz; Kf = potassium feldspar; Ab = albite; Bt = biotite; Cln = clinochlore; Plg = plagioclase; Grt = garnet; And = andalusite; Sill = sillimanite.

metamorphic apatite are generally low (Nash, 1984), a Ba analogue of chlorapatite coexisting with pure fluorapatite occurs in metamorphosed evaporites (Newberry et al., 1981). No TEM work was attempted to see whether there was such coexistence in our sample; rather, the apatite was assumed to be homogeneous.